ENCIT 2018

ABCM Associação Brasileira de Engenharia e Ciências Mecânicas

17th Brazilian Congress of Thermal Sciences and Engineering
November 25th-28th, 2018, Águas de Lindóia, SP, Brazil

ENCIT-2018-0447
Fractional calculus applied to linear thermoacoustics: A generalization of Rott's model

Carlos Alberto Valentim Junior
University of Campinas (UNICAMP), School of Mechanical Engineering, Campinas, Brazil
valentim.biossistemas@gmail.com

Flávio de Campos Bannwart
University of Campinas (UNICAMP), School of Mechanical Engineering, Campinas, Brazil
fcbannwart@fem.unicamp.br

Sergio Adriani David
University of São Paulo (USP), Department of Biosystems Engineering, Pirassununga, Brazil
sergiodavid@usp.br

Abstract. *Thermoacoustic engines are often investigated as viable alternatives for energy regeneration. The most widely used analytical model for pressure wave propagation in thermoacoustic devices is the second order linear model developed by Nikolaus Rott. In this work, we propose a generalization of Rott's equation under the regard of fractional order calculus; we also propose a solution for this generalized equation for a specific domain. Simulations of thermoacoustic engines verify this solution and indicate potential advantages of a continuously variable order, adjustable with experimental data, as it may cover nonlinearities and effects of geometrical complexities present in test rigs. Therefore, the resulting model may better fit real systems, which leads to more accurate designing.*

Keywords: *fractional calculus, thermoacoustics, energy regeneration.*

1. INTRODUCTION

Thermoacoustic engines are devices that convert thermal into mechanical energy by means of acoustic oscillations in gaseous media sustained by a sufficiently high temperature gradient, usually provided along a porous material (Rott, 1980). They are often considered for research as a viable solution for energy regeneration because of their inherent capacity of harnessing energy from low-grade heat sources (Yang *et al.*, 2018; Gardner and Howard, 2009). Those machines have other advantages, such as their high reliability due to the absence of moving parts and being able of operating not constrained by phase shifting in its working gas (de Blok, 2010), making it a standout among other mechanisms. Thermoacoustic machines can either be refrigerators or engines, depending on the direction of the energy flux (Bannwart and Arruda, 2009).

In the case of engines, the acoustic power is produced when a sufficiently high temperature gradient is kept along the internal walls of a porous material and a thermoacoustic effect takes place. Either standing or traveling waves can be generated, depending on the configuration of the waveguide network. For each kind of acoustic field a proper porous material shall be employed (Swift, 2002). The engines operating under the standing wave regime are generally less efficient and the acoustic particle approaches the Brayton cycle, whereas under the traveling wave regime the efficiency is improved due to the Stirling cycle approximation.

The most important features that affect the acoustic power produced by thermoacoustic engines are geometry, porous material, working gas conditions, and temperature profile. Recent investigations have achieved configurations that yield better performance, including optimal operating frequency and characteristics of the porous material (Bannwart *et al.*, 2013; Bannwart, 2014; Arafa *et al.*, 2011), usually employing the linear model developed by Rott (1969). Although reliable, this model can be limiting when modeling high pressure oscillations, once its equations are derived through a linear acoustic approximation (Swift, 1992).

In this work, we propose the use of fractional calculus for generalizing Rott's model. The subject, which is also called arbitrary order calculus, is a branch of mathematics that functions as a generalization of integer order calculus, in which derivatives and integrals can assume non-integer and even complex orders (Oldham and Spanier, 1974; Herrmann, 2014). Until recently, it was a tool used only by mathematicians, but this fact has been steadily changing due to the development and good applicability of the subject to several areas (David *et al.*, 2011). These perspectives motivated

us to seek in the fractional calculus a possibility of improvement of Rott's model, specially because the tool has been effective in describing diffusive and oscillatory phenomena (Agrawal, 2002; David and Valentim, 2015). The idea is that a model with non-integer orders can capture some of the non-linear behavior that the traditional model fails to represent. Besides, the arbitrary order works as an extra parameter for fitting, allowing a more faithful representation of experimental data (David *et al.*, 2016).

Thus, we derive and propose a solution for the generalized Rott's differential equation using fractional calculus. As a continuation of the work presented by Valentim *et al.* (2017), we also simulate the behavior of a complete standing wave thermoacoustic engine using this generalized solution and verify it against the usual analytical integer order solution. This procedure is used to verify the proposed solution, since the generalized model should recover the traditional model for the arbitrary order $\alpha = 1$. We also evaluate the behavior of the model for $\alpha < 1$ and discuss potential advantages of this extra parameter.

2. PROBLEM MODELING

2.1 Rott's linear thermoacoustics

Nikolaus Rott (1969) proposed the model here described by Eq. (1), where $\tilde{p}(x)$ is the complex acoustic pressure in the longitudinal direction x along a porous channel. The propagative wave is considered plane and the absolute pressure of the acoustic particle is given by $p(x,t) = p_m + Re[\tilde{p}(x)e^{-i\omega t}]$, where p_m represents the mean pressure inside the thermoacoustic device.

$$\frac{d^2\tilde{p}}{dx^2} + \left[\left(1 - \frac{1}{1-f_\nu}\frac{f_\kappa - f_\nu}{1-\sigma}\right)\frac{1}{T_m}\frac{dT_m}{dx} - \frac{1}{1-f_\nu}\frac{df_\nu}{dx}\right]\frac{d\tilde{p}}{dx} + \frac{\omega^2}{c_0^2}\frac{[1+(\gamma-1)f_\kappa]}{1-f_\nu}\tilde{p} = 0, \tag{1}$$

where T_m is the cross-sectional mean temperature, σ is the Prandtl Number, ω is the angular frequency, c_0 is the speed of sound, and γ is the polytropic coefficient. The functions f_ν and f_κ account for losses regarding viscous dissipation and thermal relaxation, respectively (Swift, 2002). The latter are calculated as functions of the working gas thermophysical properties and the channel geometry, either for the waveguide or the pore of the stack (in this work both are considered cylindric).

Equation (1) can be written in a generalized form by exchanging the derivatives $\frac{d}{dx}$ and $\frac{d^2}{dx^2}$ for D^α and $D^{2\alpha}$, which are operators of derivatives of arbitrary orders, as shown in Eq. (2). The model is analyzed for values of $0.5 < \alpha \leq 1$, which means that the arbitrary orders must be within the interval of $1 < 2\alpha \leq 2$. Thus, α may be 1, recovering the original Rott's equation, or may be fractional, providing the model an additional parameter that can be adjusted according to the scenario being modeled.

$$D^{2\alpha}\tilde{p} + \left[\left(1 - \frac{1}{1-f_\nu}\frac{f_\kappa - f_\nu}{1-\sigma}\right)\frac{1}{T_m}\frac{dT_m}{dx} - \frac{1}{1-f_\nu}\frac{df_\nu}{dx}\right]D^\alpha\tilde{p} + \frac{\omega^2}{c_0^2}\frac{[1+(\gamma-1)f_\kappa]}{1-f_\nu}\tilde{p} = 0. \tag{2}$$

2.2 Solution of the generalized model

There are manifold approaches usable to define the fractional derivative represented by the operator D^α, each one having its own advantages and applications (Capelas de Oliveira and Machado, 2014; Herrmann, 2014; Oldham and Spanier, 1974). In this work the left-handed Caputo (1967) definition is used, represented by Eq. (3), because it can treat boundary conditions in a similar way as integer order problems, which is convenient when modeling physical phenomena. In the aforementioned equation Γ is the gamma function, I is an integral operator and ξ is a bound variable.

$$D^\alpha\tilde{p}(x) = I^{1-\alpha}\frac{d}{dx}\tilde{p}(x) = \frac{1}{\Gamma(1-\alpha)}\int_0^x (x-\xi)^{-\alpha}\frac{d\tilde{p}(\xi)}{d\xi}d\xi. \tag{3}$$

In order to find a solution for Eq. (2), the fractional power series method is used, which is based on a fractional Taylor series (Trujillo *et al.*, 1999). Using this approach, the acoustic pressure $\tilde{p}(x)$ can be represented as an infinite fractional power series centered at $x_0 = 0$

$$\tilde{p}(x) = \sum_{n=0}^{\infty} C_n x^{n\alpha}. \tag{4}$$

Moreover, the generalized equation can be represented in a shorter form as in Eq. (5), where $A(x)$ depends on $T_m(x)$ and other coefficients, and is given by Eq. (6), while k is the wavenumber taking into account thermal and viscous losses, expressed in Eq. (7).

$$D^{2\alpha}\tilde{p}(x) + A(x)D^{\alpha}\tilde{p}(x) + k^2\tilde{p}(x) = 0. \tag{5}$$

$$A(x) = \left(1 - \frac{1}{1-f_\nu}\frac{f_\kappa - f_\nu}{1-\sigma}\right)\frac{1}{T_m}\frac{dT_m}{dx} - \frac{1}{1-f_\nu}\frac{df_\nu}{dx}. \tag{6}$$

$$k^2 = \frac{\omega^2}{c_0^2}\frac{[1+(\gamma-1)f_\kappa]}{1-f_\nu}. \tag{7}$$

Considering the definition in Eq. (3) and admitting that $\tilde{p}(x)$ can be written as a power series, one can use the property (Herrmann, 2014) given by Eq. (8) and extend it from x^k to a series of $C_n x^{n\alpha}$:

$$\frac{d^\alpha}{dx^\alpha}x^k = \frac{\Gamma(1+k)}{\Gamma(1+k-\alpha)}x^{k-\alpha}. \tag{8}$$

Thus, one obtains the fractional power series for $D^{\alpha}\tilde{p}(x)$ and $D^{2\alpha}\tilde{p}(x)$ given by Eq. (9) and Eq. (10), respectively:

$$D^{\alpha}\tilde{p}(x) = \sum_{n=1}^{\infty}\frac{\Gamma(n\alpha+1)}{\Gamma[(n-1)\alpha+1]}x^{(n-1)\alpha}, \tag{9}$$

$$D^{2\alpha}\tilde{p}(x) = \sum_{n=2}^{\infty}\frac{\Gamma(n\alpha+1)}{\Gamma[(n-2)\alpha+1]}x^{(n-2)\alpha}. \tag{10}$$

Next, one can plug back Eq. (9) and Eq. (10) into Eq. (5), obtaining

$$\sum_{n=2}^{\infty}C_n\frac{\Gamma(n\alpha+1)}{\Gamma[(n-2)\alpha+1]}x^{(n-2)\alpha} + A(x)\sum_{n=1}^{\infty}C_n\frac{\Gamma(n\alpha+1)}{\Gamma[(n-1)\alpha+1]}x^{(n-1)\alpha} + k^2\sum_{n=0}^{\infty}C_n x^{n\alpha} = 0. \tag{11}$$

After writing every term of the equation under the same summation symbol and adjusting the indexes one obtains

$$\sum_{n=0}^{\infty}\left[C_{n+2}\frac{\Gamma[(n+2)\alpha+1]}{\Gamma(n\alpha+1)}x^{n\alpha} + A(x)\,C_{n+1}\frac{\Gamma[(n+1)\alpha+1]}{\Gamma(n\alpha+1)}x^{n\alpha} + k^2C_n x^{n\alpha}\right] = 0. \tag{12}$$

Hence, a recurrence equation can be found for a non-trivial solution by rearranging Eq. (12), so that the coefficients of the fractional power series are given by

$$C_{n+2} = \frac{-A(x)C_{n+1}\Gamma[(n+1)\alpha+1)] - k^2C_n\Gamma(n\alpha+1)}{\Gamma[(n+2)\alpha+1]}. \tag{13}$$

Considering the power series that represent $\tilde{p}(x)$, given by Eq. (4), the coefficients C_0 and C_1 remain unknown. They can be set by the boundary conditions of the model. Firstly, we evaluate the acoustic pressure p_0 at $x = 0$ in Eq. (14) and define the coefficient C_0 in Eq. (15).

$$\tilde{p}(0) = \sum_{n=0}^{\infty}C_n x^{n\alpha} = C_0 + 0 + 0 + 0 + \cdots = p_0. \tag{14}$$

$$C_0 = p_0. \tag{15}$$

After that, one sets that the derivative of order α of $\tilde{p}(x)$ at $x = 0$ equals the constant μ_0, as shown in Eq. (16), and completes the recurrence relations with Eq. (17) representing the coefficient C_1.

$$D^{\alpha}\tilde{p}(0) = C_1 \frac{\Gamma(\alpha+1)}{\Gamma(1)} + 0 + 0 + \cdots = \mu_0. \tag{16}$$

$$C_1 = \frac{\mu_0}{\Gamma(\alpha+1)}. \tag{17}$$

Finally, these relations are used to obtain the series approximation for $\tilde{p}(x)$

$$\begin{aligned}\tilde{p}(x) = p_0 &\left[1 - \frac{k^2}{\Gamma(2\alpha+1)}x^{2\alpha} + \frac{k^2 A(x)}{\Gamma(3\alpha+1)}x^{3\alpha} + \frac{k^2[k^2 - A(x)]}{\Gamma(4\alpha+1)}x^{4\alpha} + \ldots\right] \\ + \mu_0 &\left[\frac{1}{\Gamma(\alpha+1)}x^{\alpha} - \frac{A(x)}{\Gamma(2\alpha+1)}x^{2\alpha} + \frac{A^2(x) - k^2}{\Gamma(3\alpha+1)}x^{3\alpha} + \frac{2A(x)k^2 - A^3(x)}{\Gamma(4\alpha+1)}x^{4\alpha} + \ldots\right].\end{aligned} \tag{18}$$

3. SIMULATIONS

3.1 Implementation of the model from an experimental engine

The general solution given by Eq. (18) is simulated using the software Mathematica to model a simple standing wave thermoacoustic engine, as the one sketched in Fig. 1. The entire domain from $x = 0$ to $x = L$ is treated as several juxtaposed subsystems, in which each one has its own distinct characteristics. The wave propagation in the first segment ($0 \leq x \leq x_l$) and in the last segment ($x_w \leq x \leq L$) are analytically modeled as in simple waveguides filled only with the working gas with homogeneous mean temperature profile; the thermo-viscous losses are taken into account as shown in Eq. 7. The second and third segments have their mean temperature profile inhomogeneous the feature that defines the thermoacoustic core (TAC). The thermoacoustic phenomena take place in the TAC precisely because of that feature and, essentially, in the active part ($x_s \leq x \leq x_h$), where the porous material is present. The third segment is the passive part of the TAC ($x_h \leq x \leq x_w$), and it works as a thermal buffer tube. The thermo-viscous losses are also considered in the TAC, and they are dominant within the pore internal walls of the stack. This consideration, however, must take account of how T_m varies with x. The approach of dividing the whole domain in smaller subsystems help to maintain the series solution within its radius of convergence, and the number of terms chosen to be used in each series for all simulations, after proper investigation, resulted in 20.

The working gas used in the simulations is air at ambient temperature and pressure, as described in Tab. 1. The lengths of each part of the engine and the characteristics of the stack are presented in Tab. 2 and 3, respectively. All components of the engine, including the pores within the stack, are considered cylindrical. The values and codes of all parameters used in the simulations were taken from the works of Bannwart (2014), where the actual test rig was investigated and optimal standing and traveling wave thermoacoustic engines for different porous materials were achieved. The standing wave engine shown in Fig. 1 is one of these optimal machines.

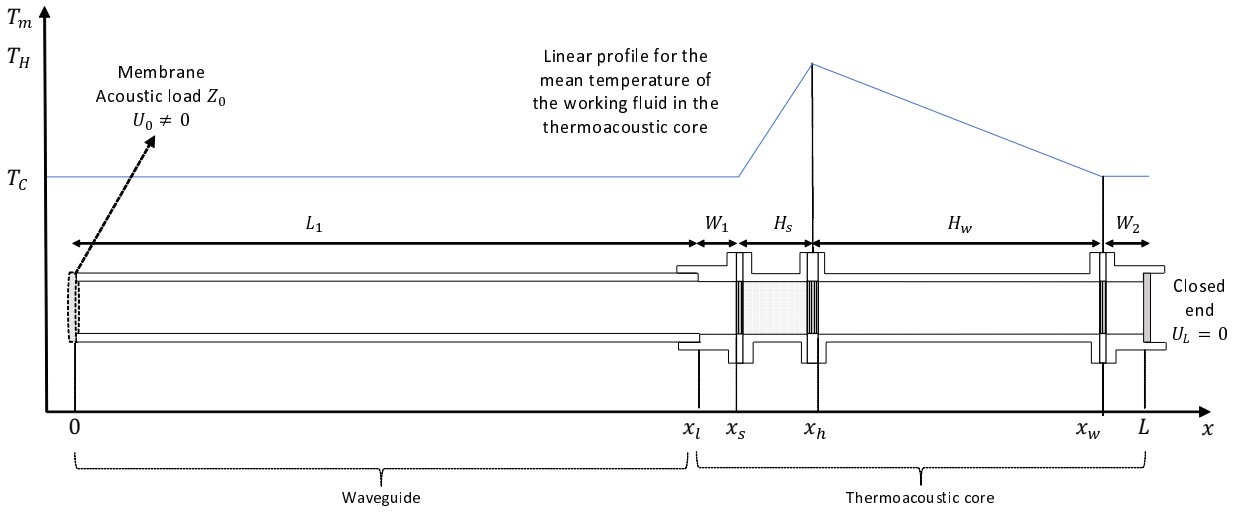

Figure 1. Schematic representation of the simulated standing wave thermoacoustic engine from Bannwart (2014).

The linear profile for $T_m(x)$ drawn in Fig. 1 is a simplified approximation of the temperature inside the TAC, and has a maximum of $T_H = 575.15$ K at the hot heat exchanger, and a minimum of $T_C = 295.15$ K, for the ambient

temperature. Even though there was not a direct measurement of the temperature inside the TAC for the regime simulated here, these parameters were estimated based on the maximal and minimal temperatures of a linear profile that would match the conditions in the work of Bannwart (2014). The value of T_H was achieved by running the model with different temperatures and choosing the one with which the model would better comply to the boundary conditions in the right extremity of the thermoacoustic engine simulated. A short stack hypothesis is admitted regarding f_κ and f_ν, with these functions being considered constants within each subsystem and calculated for the average temperature between T_H and T_C inside the core.

Figure 1 also shows the boundary conditions to be adopted in the model. On the left end, we have a membrane where the acoustic pressure is treated as a reference pressure, thus $p_0 = 1$ Pa. The membrane has an acoustic load Z_0 that represents the entry impedance of the set composed by all the elements of the thermoacoustic engine and the working gas and may be obtained analytically or experimentally. The second boundary condition μ_0 can be related to the volume velocity $\tilde{U}(x)$ of the acoustic particle by means of Eq. (19), in which S_w is the cross-sectional area of the waveguide, ρ_m is the mean density of the working gas and i is the imaginary unit. This allows us to express μ_0 by calculating the volume velocity U_0 from the impedance Z_0, since that $U_0 = p_0/Z_0$. The operation frequency used in the simulation is $f = 121$ Hz, and along with the entry impedance Z_0, was obtained experimentally by Bannwart (2014) for the specific configuration of engine used in this work.

$$\tilde{U}(x) = \frac{S_w}{i\omega\rho_m}\frac{d\tilde{p}}{dx}(1 - f_\nu). \tag{19}$$

Table 1. TAC temperatures and thermophysical properties of the air from Bannwart (2014) used in the simulations.

Parameter	Representation	Value
Hot source temperature	T_H	575.15 K
Ambient temperature	T_C	295.15 K
Mean pressure	P_m	101.9 kPa
Mean density	ρ_m	1.203 kg/m^3
Viscosity	μ	1.819×10^{-5} Pa.s
Thermal conductivity	k_{cond}	0.0260 W/(m.K)
Specific heat coefficient at constant pressure	C_P	1003 J/(kg.K)
Politropic coefficient	γ	1.402
Sound velocity at ambient temperature	c_0	344.6 m/s
Prandtl number	σ	0.7008

Table 2. Optimal thermoacoustic engine from Bannwart (2014) used in the simulations.

Parameter	Representation	Value
Waveguide	L_1	1.0600 m
First waveguide inside the core	W_1	0.0640 m
Active part of the core	H_s	0.0875 m
Passive part of the core	H_w	0.2700 m
Second waveguide inside the core	W_2	0.0540 m
Waveguide radius	R_w	0.0169 m
Waveguide cross-sectional area	S_w	8.9727×10^{-4} m^2

3.2 Simulation results

The complex pressure $\tilde{p}(x)$ and volume velocity $\tilde{U}(x)$ are analyzed within the domain $0 \leq x \leq L$ and are given in Pa and m^3/s, respectively. Figures 2, 3 and 4 show a comparison between the obtained analytical solution represented by Eq. (18) with $\alpha = 1$ and an interpolating function for a fourth order Runge-Kutta numerical solution for Eq. (1). The agreement between the continuous and dashed curves can be seen both for the acoustic pressure and the volume velocity, which verifies the generalized solution for $\alpha = 1$.

Table 3. Geometrical parameters of the Ceramic Catalyst from Bannwart (2014) used in the simulations.

Parameter	Representation	Value
Radius of the pore of the ceramic material	R_p	5.33×10^{-4} m
Porosity	ϕ	0.83
Free cross-sectional area of the stack	S_s	7.45×10^{-4} m^2

Analyzing the acoustic pressure and the volume velocity for the integer case in these figures, one can see that the acoustic pressure has its peaks at the extremities of the engine, while the volume velocity is greater at the medium portion, as expected for standing wave engines. At $x = L$ the phase difference between $\tilde{p}$ and $\tilde{U}$ approaches $\pi/2$, while at $x = 0$ they are in phase, which is consistent with the fact that there is a rigid wall (no energy flux) at $x = L$ and an acoustic load (or acoustic power production) at $x = 0$. In every figure the vertical dashed lines mark the delimitations of the active and passive parts of the TAC, as indicated in Fig. 1. In the active part, one can see that the increase in viscous resistance caused by the ceramic material drastically changes pressure and velocity. The point where the hot heat exchanger is located ($x = x_h$) also has an impact in the volume velocity due to the rise of sound speed with temperature. The acoustic power presented in Fig. 4 is calculated by the relation of real and imaginary parts of the acoustic pressure and velocity. It can be seen that the power produced in the core is negative, which means that it propagates against the direction chosen for x, with a portion of it being dissipated until it reaches the acoustic load, here represented by a membrane.

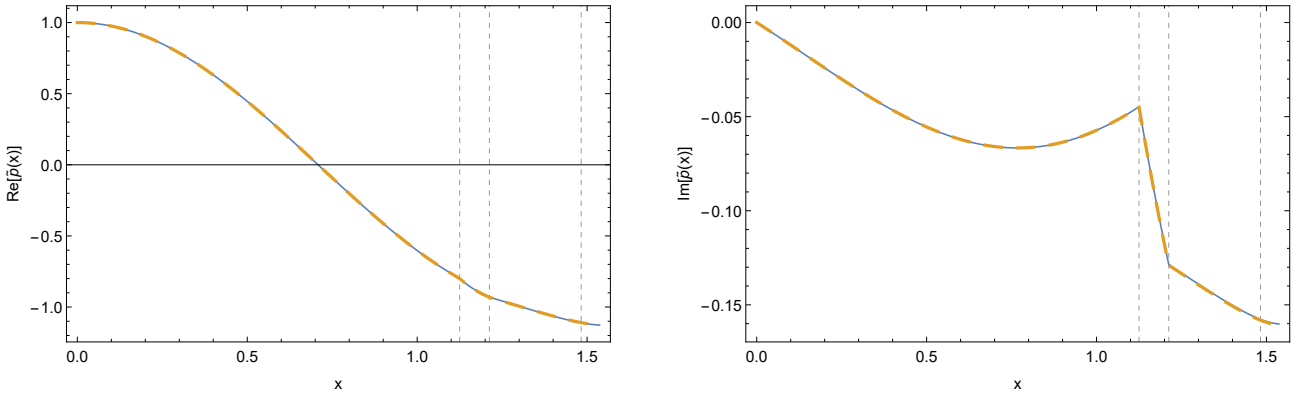

Figure 2. Real (left) and imaginary (right) acoustic pressure for the generalized solution. Comparison between the obtained solution with $\alpha = 1$ (continuous blue line) and fourth order Runge-Kutta approximation (dashed orange line).

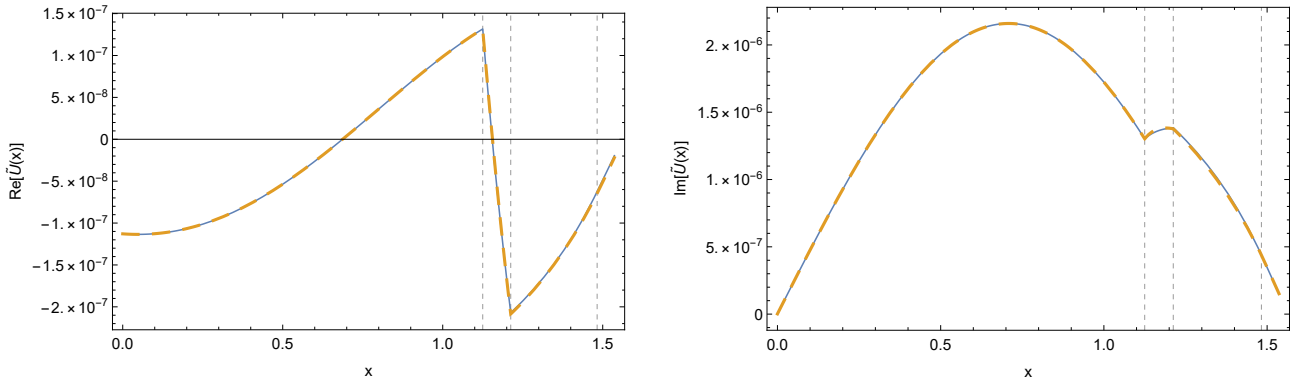

Figure 3. Real (left) and imaginary (right) volume velocity for the generalized solution. Comparison between the obtained solution with $\alpha = 1$ (continuous blue line) and fourth order Runge-Kutta approximation (dashed orange line).

When Eq. (18) is simulated for different values of α, one can see a change in the amplitudes and in the position of the nodes of the curves for both real and imaginary parts and magnitudes of the acoustic pressure and the volume velocity, represented by Figs. 5, 6 and 7. The models with $\alpha < 1$ seem to have dissipative effects that become more pronounced as the values of α get smaller. This feature can be interpreted as an advantageous factor of Eq. (18) for fitting experimental data, since α can be treated as a continuous adjustable extra parameter for the model.

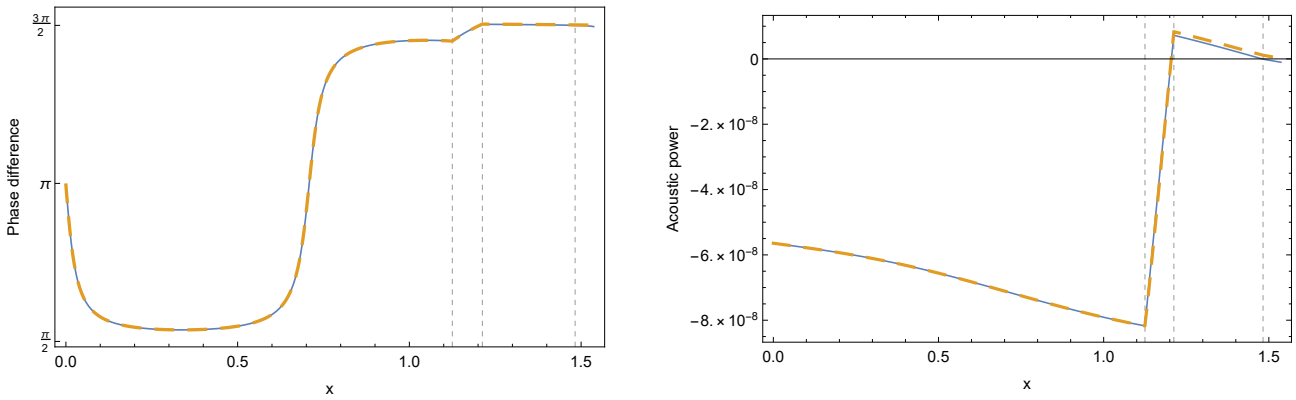

Figure 4. Phase difference between acoustic pressure and volume velocity (left) and acoustic power (right). Comparison between the obtained solution with $\alpha = 1$ (continuous blue line) and fourth order Runge-Kutta approximation (dashed orange line).

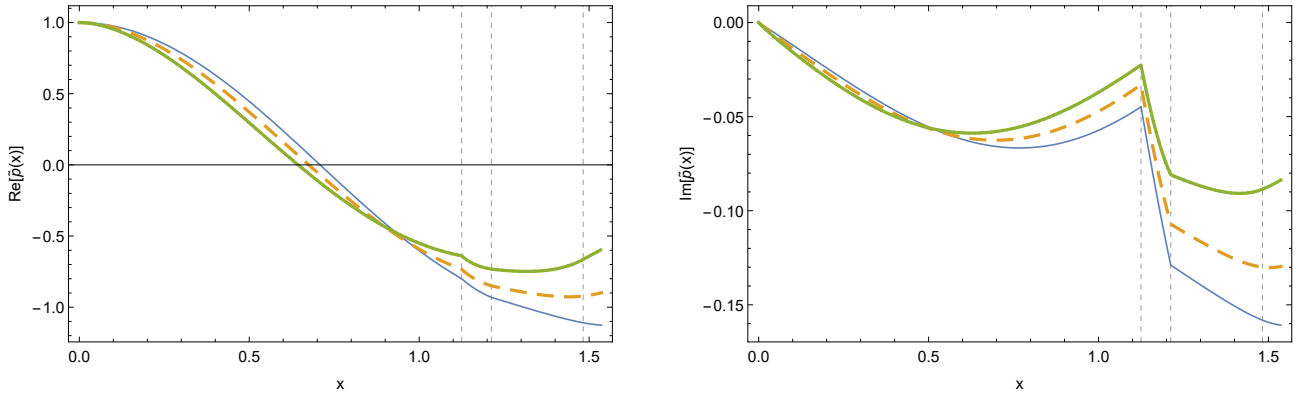

Figure 5. Real (left) and imaginary (right) acoustic pressure for the generalized solution. Comparison between models with $\alpha = 1$ (continuous blue line), $\alpha = 0.95$ (dashed orange line) and $\alpha = 0.9$ (thicker green line).

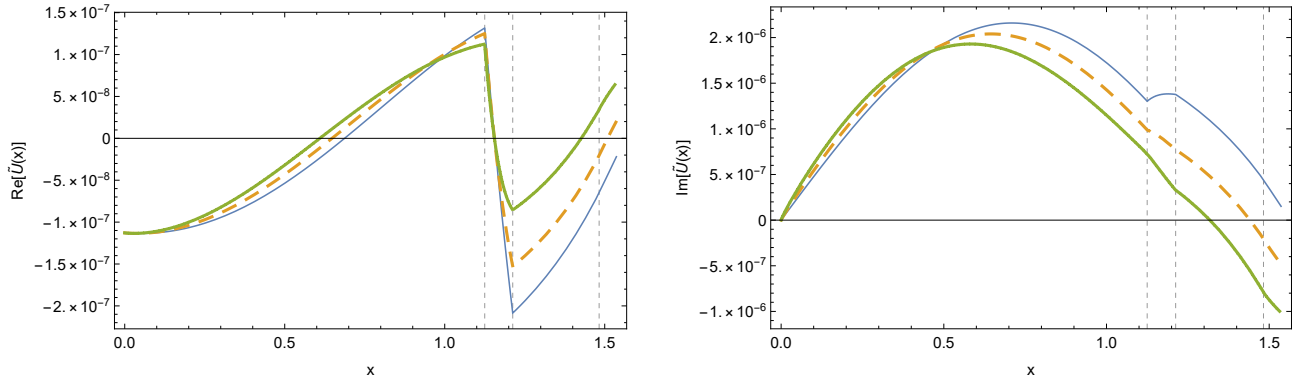

Figure 6. Real (left) and imaginary (right) volume velocity for the generalized solution. Comparison between models with $\alpha = 1$ (continuous blue line), $\alpha = 0.95$ (dashed orange line) and $\alpha = 0.9$ (thicker green line).

4. CONCLUSIONS

In this work, we proposed a generalization of the linear equation for pressure propagation in thermoacoustics developed by Rott (1969). The general solution was achieved through the method of fractional power series. When the arbitrary order α is equal to one, an expression equivalent to the original solution of Rott's equation is obtained, which is verified in two ways: physically, through the plausible behavior of the acoustic pressure and volume velocity curves for the acoustic particle within the thermoacoustic engine; and mathematically, by comparing the obtained solution to a fourth order Runge-Kutta approximation. For the simulations with $\alpha < 1$, the pressure and velocity curves obtained presented accentuated dissipative behaviors, which is in agreement to other studies regarding generalized wave-like equations (Agrawal, 2002). Under those circumstances, α can be interpreted as an analytical parameter that can be adjusted to fit the obtained solution to experimental data. This feature allows to cover eventual nonlinearities without the need to

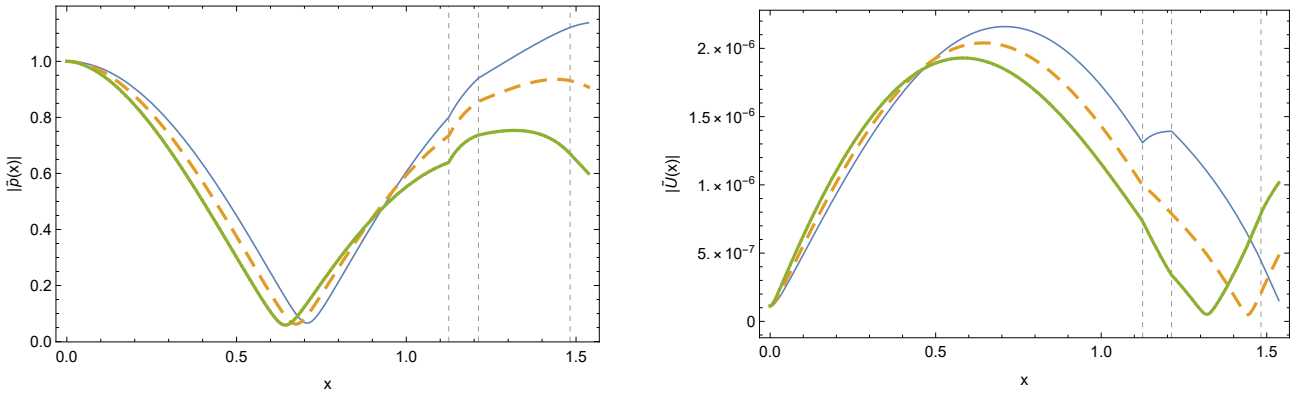

Figure 7. Magnitudes of acoustic pressure (left) and volume velocity (right) for the generalized solution. Comparison between models with $\alpha = 1$ (continuous blue line), $\alpha = 0.95$ (dashed orange line) and $\alpha = 0.9$ (thicker green line).

understand their causes, as they are implicitly included in this adjustment. As a continuation of this work, the fractional model, in principle, can then be used to predict the behavior of this thermoacoustic engine for other working conditions, not demanding further experimental characterizations. That would completely fulfill the natural purpose of fractional modeling. In parallel, another subsequent work would be to generalize the model even further by changing the operator $D^{2\alpha}$ to D^{β}, thus eliminating the dependence between the orders of the operators and extending the coverage of the model.

5. ACKNOWLEDGMENTS

This work was conducted during a scholarship supported and financed by CAPES - Brazilian Federal Agency for Support and Evaluation of Graduate Education within the Ministry of Education of Brazil.

6. REFERENCES

Agrawal, O.P., 2002. "Solution for a fractional diffusion-wave equation defined in a bounded domain". *Nonlinear Dynamics*, Vol. 29, No. 1-4, pp. 145–155. ISSN 0924090X. doi:10.1023/A:1016539022492.

Arafa, N., Ibrahim, A.H., Addas, K. and Abdel-rahman, E., 2011. "Design Considerations for Thermoacoustic Engines for Low Onset Temperature and Efficient Operation". In *Forum Acusticum*. European Acoustics Association, Aalborg, Denmark, Vol. 27, pp. 961–966. ISBN 978-84-694-1520-7. ISSN 2221-3767.

Bannwart, F.C., 2014. *Methods for the transfer matrix evaluation of thermoacoustic cores with application to the design of thermoacoustic engines*. Ph.D. thesis, Université du Maine / Unicamp.

Bannwart, F.C. and Arruda, J.R.F., 2009. "Construction of a Demonstrative Apparatus for the Thermoacoustic Refrigeration Effect Construction of a Demonstrative Apparatus for the Thermoacoustic". In *Proceedings of the XIII International Symposium on Dynamic Problems of Mechanics*. ABMC, Angra dos Reis, RJ, Brazil.

Bannwart, F.C., Penelet, G., Lotton, P. and Dalmont, J.P., 2013. "Measurements of the impedance matrix of a thermoacoustic core: applications to the design of thermoacoustic engines." *The Journal of the Acoustical Society of America*, Vol. 133, No. 5, pp. 2650–60. ISSN 1520-8524. doi:10.1121/1.4796131.

Capelas de Oliveira, E. and Machado, J.A.T., 2014. "A review of definitions for fractional derivatives and integral". *Mathematical Problems in Engineering*, Vol. 2014, No. 1940. ISSN 15635147. doi:10.1155/2014/238459.

Caputo, M., 1967. "Linear Models of Dissipation whose Q is almost Frequency Independent II". *Geophysical Journal International*, Vol. 13, No. 5, pp. 529–539. doi:10.1111/j.1365-246X.1967.tb02303.x.

David, S.A., Linares, J.L. and Pallone, E., 2011. "Fractional order calculus: historical apologia, basic concepts and some applications". *Revista Brasileira de Ensino de Física*, Vol. 33, No. 4, pp. 4302–4302. ISSN 1806-1117. doi: 10.1590/S1806-11172011000400002.

David, S.A., de Sousa, R.V., Valentim, C.A., Tabile, R.A. and Machado, J.A.T., 2016. "Fractional PID controller in an active image stabilization system for mitigating vibration effects in agricultural tractors". *Computers and Electronics in Agriculture*, Vol. 131, pp. 1–9. ISSN 01681699. doi:10.1016/j.compag.2016.11.001.

David, S.A. and Valentim, C.A., 2015. "Fractional Euler-Lagrange Equations Applied to Oscillatory Systems". *Mathematics*, Vol. 3, No. 2, pp. 258–272. ISSN 2227-7390. doi:10.3390/math3020258.

de Blok, K., 2010. "Novel 4-Stage Traveling Wave Thermoacoustic Power Generator". In *ASME 2010 3rd Joint US-European Fluids Engineering Summer Meeting collocated with 8th International Conference on Nanochannels, Microchannels, and Minichannels*. American Society of Mechanical Engineers, Montreal, Canada, pp. 73–79.

Gardner, D.L. and Howard, C.Q., 2009. "Waste-Heat-Driven Thermoacoustic Engine and Refrigerator". In *Acoustics*. Adelaide, Australia, November, pp. 23–26. ISBN 9780975785577.

Herrmann, R., 2014. *Fractional calculus: An introduction for physicists*. World Scientific, Singapore, 2nd edition. ISBN 978-981-4551-09-0. doi:10.1142/8934.

Oldham, K.B. and Spanier, J., 1974. *The fractional calculus - theory and applications of differentiation and integration to arbitrary order*. Academic Press, New York.

Rott, N., 1969. "Damped and Thermally Driven Acoustic Oscillations in Wide and Narrow Tubes". *Journal of Applied Mathematics and Physics (ZAMP)*, Vol. 20, No. 1, pp. 230–243.

Rott, N., 1980. "Thermoacoustics". *Advances in Applied Mechanics*, Vol. 20, pp. 135–175. ISSN 00652156. doi: 10.1016/S0065-2156(08)70233-3.

Swift, G.W., 1992. "Analysis and performance of a large thermoacoustic engine". *The Journal of the Acoustical Society of America*, Vol. 92, No. 3, pp. 1551–1563. ISSN 0001-4966. doi:10.1121/1.403896.

Swift, G.W., 2002. *Thermoacoustics: A unifying perspective for some engines and refrigerators*. Acoustical Society of America, Melville, NY, 1st edition. ISBN 0-7354-0065-2.

Trujillo, J.J., Ribero, M. and Bonilla, B., 1999. "On a Riemann-Liouville Generalized Taylor's Formula". *Journal of Mathematical Analysis and Applications*, Vol. 231, pp. 255–265.

Valentim, C.A., Bannwart, F.C. and David, S.A., 2017. "Fractional order calculus applied to generalize the Rott's linear thermoacoustics: an investigation toward energy regeneration in automobiles". In *24th ABCM International Congress of Mechanical Engineering*. ABCM, Curitiba, PR, Brazil., December, pp. 1–8. doi: 10.26678/ABCM.COBEM2017.COB17-1082.

Yang, R., Wang, Y., Jin, T., Feng, Y. and Tang, K., 2018. "Development of a three-stage looped thermoacoustic electric generator capable of utilizing heat source below 120 C". *Energy Conversion and Management*, Vol. 155, pp. 161–168. ISSN 01968904. doi:10.1016/j.enconman.2017.10.084.

7. RESPONSIBILITY NOTICE

The authors are the only responsible for the printed material included in this paper.